John von Neumann Institute for Computing

Accessing the Dynamics of Strongly-Correlated Many Body Systems within the Operator Loop Update and its Application to High-Temperature Superconductivity

Ansgar Dorneich, Martin Jöstingmeier, Enrico Arrigoni,
Werner Hanke, Matthias Troyer

published in

NIC Symposium 2004, Proceedings,
Dietrich Wolf, Gernot Münster, Manfred Kremer (Editors),
John von Neumann Institute for Computing, Jülich,
NIC Series, Vol. **20**, ISBN 3-00-012372-5, pp. 227-239,3 2003.

http://www.fz-juelich.de/nic-series/volume20

Accessing the Dynamics of Strongly-Correlated Many Body Systems within the Operator Loop Update and its Application to High-Temperature Superconductivity

Ansgar Dorneich[1] **, Martin Jöstingmeier**[1] **, Enrico Arrigoni**[1] **, Werner Hanke**[1]**, and Matthias Troyer**[2]

[1] Inst. f. Theoretische Physik, Am Hubland, 97074 Würzburg, Germany
E-mail: {ardornei, joesel}@physik.uni-wuerzburg.de
arrigoni@itp.tu-graz.ac.at, hanke@physik.uni-wuerzburg.de

[2] Theoretische Physik, ETH Zürich, 8093 Zürich, Switzerland
E-mail: troyer@itp.phys.ethz.ch

We present an algorithm for measuring arbitrary one-particle Greens functions within the operator loop update mechanism. Further this method is applied to the the $pSO(5)$model of high-temperature superconductivity and we present its three dimensional the phase diagram. Within the parameter regime studied we show that the model under consideration reproduces salient features of the cuprates phase diagram and that $SO(5)$symetry is restored in a transient regime, although $SO(5)$symetry is broken at the hamiltonian level.

1 Introduction

Strongly-correlated electron systems rank amongst the most intensively studied objects in modern theoretical solid state physics[1–9]. The reason for this interest is that strongly interacting electrons are the key ingredient for many exotic optical, electrical and magnetic properties of technologically promising materials such as high-temperature superconductors (HTSC)[10] or colossal magneto-resistance materials (CMR)[2]. Amongst many others, possible applications for these classes of materials range from magnetic data recording to dramatically faster computers, loss-free transport and storage of electrical energy, new means of public transport based on magnetic levitation, medical imaging, better speech quality in mobile communication, and hyperfine detectors in scientific research and material testing.
Numerical simulations have become important tools within solid state physics, and are a substantial part of the literature and ongoing works in this area rely on these 'computer experiments'[1,11,12]. Numerical simulations allow measurements of the properties of well defined microscopic model Hamiltonians up to essentially arbitrary accuracy, thereby taking into account all quantum mechanical interactions without any approximation or perturbation expansion. However numerical simulation techniques must still be further developed, because they suffer from the limited system sizes achievable, i.e. with the Lanczos algorithm ≈ 20 sites, with Quantum–Monte Carlo (QMC) methods $\approx 10^2$ sites for fermionic systems and $\approx 10^4$ sites for bosonic systems, which is far away from thermodynamic limit of about 10^{13} atoms in a cube of 1cm^3 of a real solid .

In this paper, we first review a QMC method, the so called Stochastic Series Expansion (SSE) and further present an extension of the loop–operator update, wich allows to access arbitrary one–particle green's functions within the numerically exact SSE technique

(see Sec.2). Section 3 is dedicated to an up-to-date application of the developed program package: The projected-SO(5) ($pSO(5)$) model in three dimensions which is a promising theory for HTSC. In section 4, we summarize our work.

2 The SSE Technique and the Update Mechanism

QMC techniques are currently the most important simulation tools of strongly-correlated solid-state physics. Many different variants have been developed, and we refer to reference 13 for an overview. The basic idea of all these variants is instead of using *all* basis states of the Hilbert space for exactly diagonalizing the measurement operators, but to calculate statistical mean values of the measurable quantity based on a relatively small ensemble of the 'statistically most relevant' states of the system. These states are sampled starting from an arbitrarily chosen initial state and using a statistical sampling process. The statistical process has to be organized in such a way that the correct thermodynamics of the system studied is captured: i.e. each state s should be sampled with a probability, which is proportional to its Boltzmann factor $\mathrm{e}^{-E(s)/k_BT}$ (Ref. 14, 15). It can be shown[14] that this is guaranteed if the process fulfills the *detailed balance* criterion. Unlike ED and DMRG (apart from some rather involved extensions to $T>0$), it also works at finite temperature, thus providing access to thermodynamical properties of the system. The central quantity to be sampled in a QMC simulation is the partition function, i.e.

$$Z = \mathrm{Tr}(\mathrm{e}^{-\beta\hat{H}}), \tag{1}$$

where $\hat{H}$ is the system's Hamiltonian and $\beta = 1/T$ the inverse temperature. Standard QMC techniques[13] split up the exponential into a product of many 'imaginary time slices' $\mathrm{e}^{-\Delta\tau\hat{H}}$ and truncate the Taylor expansion of this expression after a certain order in $\Delta\tau$, thereby introducing a discretization error of order $(\Delta\tau)^n$.
In SSE, however, one chooses a convenient Hilbert base $\{|\,\alpha\rangle\}$ and expands Z into the power series

$$Z = \sum_{\alpha}\sum_{n=0}^{\infty}\frac{(-\beta)^n}{n!}\langle\alpha\,|\hat{H}^n|\,\alpha\rangle. \tag{2}$$

It can be shown that the statistically relevant exponents of this power series are centered around

$$\langle n\rangle \propto N_s\beta, \tag{3}$$

where N_s is the number of sites (or orbitals) in the system[16]. We can, thus, truncate the infinite sum over n at a finite cut-off length $L \propto N_s\beta$ without introducing any systematic error for practical computations. The best value for L can be determined and adjusted during an initial thermalization phase of the QMC simulation: beginning with a relatively small value of L, one can start the QMC update process, stop it whenever the cut-off L is exceeded and restart with L increased by 10 to 20%. Now let $\hat{H}$ be composed of a certain number of elementary interactions involving one or two sites (such as on-site potentials, nearest neighbor hopping etc.). In order to obtain a uniform notation, we combine those interactions, affecting only a single site to new 'bond' interactions. One can, for example, take two chemical potential terms $\mu\cdot\hat{n}$(site1) and $\mu\cdot\hat{n}$(site2) and form the bond term

$\frac{1}{C}\mu(\hat{n}(\text{site1}) + \hat{n}(\text{site2}))$ with the constant C assuring that the sum over all new bond terms equals the sum over all initial on-site terms. We can thus assume in the following that $\hat{H}$ is a finite sum of bond terms $\hat{H}_b$ and that the operator strings $\hat{H}^n$ in (2) can be split into terms of the form

$$\prod_{i=1}^{n} \hat{H}_{b_i}^{(a_i)}, \tag{4}$$

where b_i labels the bond on which the elementary interaction term operates and a_i the operator type (e.g. density–density interaction or hopping). By introducing "empty" unit operators $\hat{H}^{(0)} = \mathbb{1}$, one can artificially grow all operator strings to length L and then obtains[16]

$$Z = \sum_{\alpha} \sum_{\{S_L\}} \frac{\beta^n (L-n)!}{L!} \langle \alpha \mid \prod_{i=0}^{L} (-\hat{H}_{b_i}^{(a_i)}) \mid \alpha \rangle. \tag{5}$$

Here, $\{S_L\}$ denotes the set of all concatenations of L bond operators $\hat{H}_b^{(a)}$ and n is the number of non-unit operators in S_L.
If we want to sample the (α, S_L) configurations according to their relative weights with a Monte-Carlo procedure, we have to make sure that the energy of each bond operator is zero or negative since, in order to fulfill detailed balance, we choose the acceptance probability p of a bond interaction to be proportional to its negative matrix element. This requires, however, that all matrix elements are non-positive. Having outlined the basic idea of SSE, we next review the non-local updating scheme.

The basic idea was proposed by Sandvik[17]. However, we added a couple of extensions. In particular, we formulated the access and computability of time-dependent Green's functions (see Eq. (8))[18]. These Green's functions are the tools to extract the experimentally accessible information, such as the response to an external perturbation. A world-line representation is used, in which the x-axis represents the spatial dimensions and the y-axis the propagation level $l = 1...L$. We symbolize type-1 bosons by single solid lines, type-2 bosons by double lines and empty sites by dotted lines (see Fig. 1, left). Following Sandvik, we separate the set of all bond operators into three classes: empty operators $\hat{H}^{(0)} = \mathbb{1}$, diagonal operators $\hat{H}^{(d)}$ and non-diagonal operators $\hat{H}^{(nd)}$. The QMC process starts with an arbitrarily chosen initial state $\mid \alpha \rangle$ and an empty operator string: in Fig. 1 (left), for example, three sites are occupied with type-1 bosons, two sites are empty and site 2 is occupied by a type-2 particle. Now two different update steps are performed in alternating order: a diagonal update, exchanging empty and diagonal bond operators, and an operator loop update, transforming and exchanging diagonal and non-diagonal operators.
In the diagonal update step, the operator string positions $l = 1...L$ are traversed in ascending order. If the current bond operator is a non-diagonal one, it is left unchanged; if it is an empty or diagonal operator, it is replaced by a diagonal or empty one, with a certain probability satisfying detailed balance, i.e. an operator with lower energy is more likely to be maintained or inserted than an operator with higher energy (Fig. 1 middle).
Non-diagonal bond operators cannot simply be inserted into the world-line configuration as diagonal operators can: their insertion and modification requires local changes of the world-line occupations. Sandvik proposed the following method to construct such a loop:

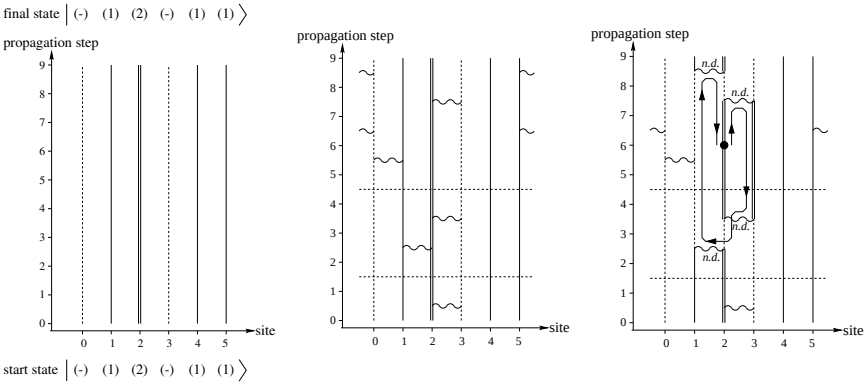

Figure 1. **Left:** *world-line representation of an arbitrarily chosen start state for a physical system with three allowed occupations per site: empty (dashed line), particle 1 (solid line) or particle 2 (double line). The initial cut-off length L has been set to $L = 9$, and the initial bond-operator string consists only of "empty" operators.* **Middle:** *in the diagonal update step a certain number of empty bond operators is replaced by diagonal ones (and vice versa). In this example 7 of the initial 9 empty operators have been replaced.* **Right:** *The loop update closes if the initial insertion point – here the propagation level 6 at world line 2 – is reached again and if the inserted world-line discontinuity is removed in this step.*

a certain world-line and a propagation level l on it is chosen arbitrarily; at the chosen point one disturbs the world-line by a local change – for example the creation or annihilation of a particle. Then one chooses a direction (up or down in propagation direction) and starts moving the disturbance in this direction. The aim is to move this disturbance (we'll call it 'loop head') through the network of world-lines and interaction vertices until the initial discontinuity is reached again and healed. Whenever the loop head reaches an interaction vertex, we must decide how to go on, satisfying detailed balance. Using this scheme a wide range of quantum mechanical observables are easily accessible by this operator loop update, for example $\langle E\rangle, C_V$ or equal time correlation functions $\langle \hat{D}_1 \hat{D}_2\rangle$ of two diagonal operators $\hat{D}_1, \hat{D}_2$.

In SSE the propagation index l describes the evolution of an initial state, when a series of elementary terms of the Hamiltonian is acting on it; thus l plays a role analogous to imaginary time in a standard path integral. More detailed calculations[19,20] show that an imaginary time separation τ corresponds to a binomial distribution of propagation distances Δl; the time-dependent correlation $\langle \hat{D}_2(\tau)\hat{D}_1(0)\rangle$, for example, is related to the correlator

$$C_{12}(\Delta l) = \frac{1}{n}\sum_{l=0}^{n-1} d_2[l+\Delta l]\, d_1[l] \tag{6}$$

via

$$\langle \hat{D}_2(\tau)\hat{D}_1(0)\rangle = \left\langle \sum_{\Delta l=0}^{n} \binom{n}{\Delta l} \left(\frac{\tau}{\beta}\right)^{\Delta l} \left(1-\frac{\tau}{\beta}\right)^{n-\Delta l} C_{12}(\Delta l) \right\rangle . \tag{7}$$

The observables listed above serve to access important static thermodynamic properties of the system studied. However, properties such as photo-emission, described by the Green's function $\langle a^{\dagger}{}_{(\mathbf{k},\omega)}\, a_{(0,0)}\rangle$, where $a_{(\mathbf{k},\omega)}$ $\left(a^{\dagger}{}_{(\mathbf{k},\omega)}\right)$ creates a hole (electron) with momentum $\vec{k}$ end energy ω, or spin flip response functions $\langle S^{-}{}_{(\mathbf{k},\omega)}\, S^{+}{}_{(0,0)}\rangle$, where S^{-} and S^{+} are the spin flip operators known from standard quantum-mechanics, are often even more interesting as they provide insights into the system's dynamics. Within the framework of SSE, measuring these Green's functions $G(\mathbf{k},\omega)$ requires the insertion of local changes on certain world-lines (such as removing a particle at propagation level l_1 on world-line w_1 and re-inserting it at propagation level l_2 on world-line w_2). Performing these insertions is a highly non-trivial task, since on the one hand detailed balance must be assured. On the other hand, the whole process has to sample all distances $r = w_2 - w_1$ and all propagation differences $\Delta l = l_2 - l_1$ efficiently. Both requirements also exist for the QMC update steps between different measurements, and within SSE they are fulfilled by introducing the non-local operator loop-update mechanism. Since this update inserts and moves local changes on the network of world-lines and connecting interaction vertices, it can be used to record the corresponding Green's functions $G(\vec{r},\Delta l)$ 'on the run', while constructing the closed loop.

Efficiently accessing the system's dynamics. In this paragraph, an efficient implementation strategy for recording $G(\vec{r},\Delta l)$ and for the adjacent transformation steps, mentioned above, is presented. The transformation from propagation levels Δl to imaginary time τ requires the same weight factors as discussed earlier for diagonal correlation functions:

$$\begin{aligned} G(r,\tau) &= \sum_{\Delta l=0}^{n} \binom{L}{\Delta l} \left(\frac{\tau}{\beta}\right)^{\Delta l} \left(1-\frac{\tau}{\beta}\right)^{L-\Delta l} G(r,\Delta l) \\ &\equiv \sum_{\Delta l=0}^{L} w(\tau,\Delta l)\; G(r,\Delta l)\,, \end{aligned} \tag{8}$$

where

$$w(\tau,\Delta l) = \binom{L}{\Delta l} \left(\frac{\tau}{\beta}\right)^{\Delta l} \left(1-\frac{\tau}{\beta}\right)^{L-\Delta l}. \tag{9}$$

Working in a fixed string size representation with fixed L instead of varying n is more convenient because the binomial weight prefactors are fixed during the entire simulation and can easily be calculated once, at the beginning of the simulation.

There are several possible ways to implement the recording of $G(\vec{r},\Delta l)$ measurements and the following transformation to $G(\vec{r},\tau)$. The easiest and, at first glance, fastest way simply writes all recorded $G(\vec{r},\Delta l)$ data into a two-dimensional array with dimensions N_s and $L \propto N_s\beta$. The transformation to $G(\vec{r},\tau)$ can then be performed at the end of the simulation. However, this method has two problems. First a separate measurement has to be recorded each time the loop head steps up or down by one level on a world-line and, whenever it traverses an interaction vertex. Recording all these measurements drastically slows down the loop update process. Second, for large systems ($N_s \approx 5000$) and low temperatures ($\beta \approx 40$), the two-dimensional array needed to store $G(\vec{r},\Delta l)$ contains about one billion elements and needs more memory than available on many computer systems. In our code we have adopted a different strategy to overcome these problems: we perform

all possible $G(\vec{r}, \Delta l)$ measurements (thereby exploiting the fact that $G(\vec{r}, \Delta l)$ is constant on the entire world-line fragment between two adjacent vertices) and directly transform these into $G(\vec{r}, \tau)$ at the end of each loop update step. On the one hand, the transformation introduced after each QMC update step is necessary to keep memory requirements manageable. On the other hand the number of floating-point operations grows significantly. Simply applying Eq. (8) with its computationally expensive operations (divisions, powers, binomial coefficients, large sums), would now cost by far too much computation time. Instead, we remember that $G(\vec{r}, \Delta l)$ is composed out of a relatively small number of intervals $I =]\Delta l_{1(I)}, \Delta l_{2(I)}]$ with constant function value (Fig. 2b). Therefore, we can compute the contribution of an entire Δl-interval to $G(\vec{r}, \tau)$ in one step:

$$G(r, \tau) = \sum_I G(r, I)\big(W(\tau, \Delta l_{2(I)}) - W(\tau, \Delta l_{1(I)})\big), \tag{10}$$

where W is the "integrated weight function"

$$W(\tau, \Delta l) = \sum_{m=0}^{\Delta l} w(\tau, m). \tag{11}$$

The Δl-range in which $W(\tau, \Delta l)$ considerably differs from 0 and 1 is determined by the mean value and the standard deviation of the b distribution $w(\tau, \Delta l)$:

$$\langle \Delta l \rangle = L\frac{\tau}{\beta} \tag{12}$$

$$\sigma_{\Delta l} = \sqrt{L\frac{\tau}{\beta}\left(1 - \frac{\tau}{\beta}\right)}. \tag{13}$$

Below $(\langle \Delta l \rangle - 5\,\sigma_{\Delta l})$ the integrated weight is zero, above $(\langle \Delta l \rangle + 5\,\sigma_{\Delta l})$ it is 1 (up to an error of less than 10^{-7}). The remaining interval rarely contains more than fifty or hundred Δl-points (see Fig. 2d); these values can easily be stored after having been computed once for each τ. Thus, $W(\tau, \Delta l)$ can be calculated very rapidly with nothing but a couple of "cheap" elementary operations. For very large systems and very low temperatures the "rel-

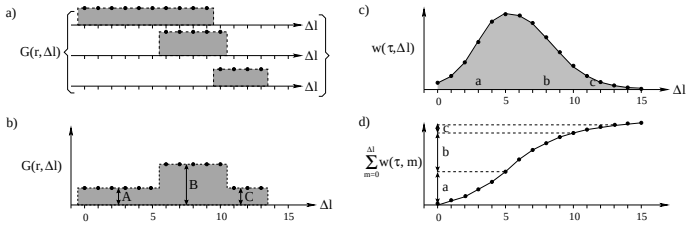

Figure 2. Transformation of Green's functions measurements from propagation level Δl to imaginary time τ: the raw measurements recorded during loop update on different world-line segments (a) are combined into a single function $G(\vec{r}, \Delta l)$ (b). For a given τ $G(\vec{r})$, could be computed by summing up all $G(\vec{r}, \Delta l)$ weighted with $w(\tau, \Delta l) = \binom{L}{\Delta l}\left(\frac{\tau}{\beta}\right)^{\Delta l}\left(1 - \frac{\tau}{\beta}\right)^{L - \Delta l}$ (c). A much more efficient way uses the "integrated weight function" $W(\tau, \Delta l) = \sum_{m=0}^{\Delta l} w(\tau, m)$ (d) to get the total contribution of each range $]\Delta l_1, \Delta l_2]$ in which $G(\vec{r}, \Delta l)$ is constanst. In the example shown here $G(\vec{r}, \tau)$ is then simply $aA + bB + cC$.

evant" Δl-ranges might become so large that it is unfavorable to store all needed $W(\tau, \Delta l)$ values – for example, because accessing the large array $W[\tau_i, \Delta l]$ would cause too many cache misses. In this case one can store the coefficients of some interpolation functions for $W(\tau, \Delta l)$ instead of the function values themselves.

The next transformation step, Fourier transform from $G(\vec{r})$ to $G(\vec{k})$, is a well-known standard method that does not impose any fundamental problems. Unlike a Fourier transform, a Laplace transform in general cannot be inverted. Therefore, the last transition step from τ to ω is by far more complicated than the previous one from r to k. We use efficient *Maximum Entropy* techniques developed within the last years and refer to earlier publications.[21]

In the next section we want to dicuss very briefly an example application, the phase diagram of the three dimensional $pSO(5)$model.

3 The pSO(5) Model of HTSC in Three Dimensions

When studying the phase diagram of high–T_c cuprates (figure (3) one notices one common feature: The close proximity of antiferromagnetism (AF) and superconductivity (SC). Both phases are states with broken symmetry: In an antiferromagnet the staggered magnetization points towards a specific direction and, therefore, breaks the SO(3) symmetry of rotational invariance in the three–dimensional space. In the superconductor, the charge conservation is broken since Cooper pairs can be freely generated from the condensate. This corresponds to a broken U(1) symmetry.

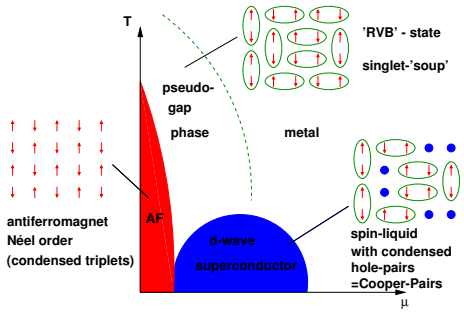

Figure 3. A generic phase diagram of high–T_c cuprates.

The two at first glance radically different states (a perfect metal i.e. superconductor on one side and an AF insulator on the other side) are both states with broken symmetry. What if the cuprates obey a higher symmetry principle than SO(3) and U(1) that is then spontaneously broken at low temperatures? This is the idea of the SO(5) symmetry principle[4,22]. SO(5) is the smallest group that combines SO(3) and U(1) (they are subgroups of SO(5)). According to this idea, the antiferromagnet and the d–wave superconductor are two aspects of a broken SO(5) symmetry state; they are "two faces of the same coin", where the chemical potential or the doping decides which face the coin "lands on".

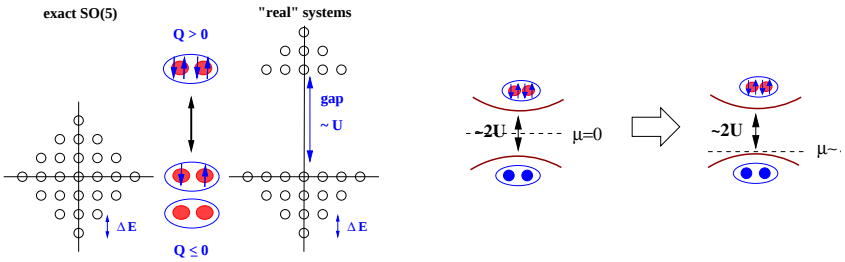

Figure 4. **Left:** In exactly SO(5)-symmetric systems collective charge and spin excitations within an SO(5) multiplet should both have vanishing energy. If exact SO(5)-symmetry is broken by a chemical potential, there are constant energy steps ΔE between adjacent Q levels (left). In physically realistic systems, however, charge excitations above half-filling must pay the large energy U due to the strong on-site repulsion of two electrons in the same orbital. **Right:** A projected SO(5) theory can account for the Mott gap and restore at least the energetic degeneracy of hole-doped and spin-excited states by shifting the chemical potential to the lower band edge. The electron pairs then become irrelevant for the low-energy description of the system due to the large Mott gap of $2U$.

3.1 The Projected $SO(5)$–Model

The SO(5) theory of HTSC, which is descibed in detail in references 4 and 22, provides an elegant explanation for many features of the cuprates such as the close vicinity of an AF and SC phases or the neutron resonance peak at $\mathbf{k} = (\pi, \pi)$[4, 23–25] and makes a number of experimental predictions[26–30]. Fingerprints of approximate SO(5) symmetry have also been detected in some widely studied microscopic effective models for the CuO_2 planes, e.g. the t-J[31] or the Hubbard model[32]. However, the cuprates' Mott insulating behavior at half-filling severely challenges the validity of SO(5) theory[33, 32, 34, 35]: SO(5) symmetry requires collective charge pair excitations to have the same (vanishing) mass as collective spin-wave excitations. The real cuprates, on the contrary, are Mott insulators at half-filling and possess a large energy gap U of several eV due to electron-electron interaction. Therefore, in physically realistic models the 'upper half' of all SO(5) multiplets, i.e. the states with $Q > 0$ ("electon doped"), should be separated from the lower part of the multiplet (holes with $Q < 0$) by the large energy difference U (see figure 4). The only way to overcome these problems is to incorporate additional SO(5)-symmetry breaking terms into the SO(5) description of the HTSC. Most important is to attain a correct description of the Mott gap at half-filling. This can be done by projecting out all states containing doubly occupied sites (i.e. the $Q > 0$ part of the SO(5) multiplets depicted in (figure 4). The resulting models, which exactly implement the so-called Gutzwiller constraint of no-double-occupancy, are called 'projected SO(5)' or 'pSO(5)' models.

3.2 A pSO(5)–Symmetric Effective Boson Hamiltonian

The natural excitations, which describe the multipletts of $SO(5)$theory and which finally give rise to the AF and SC states are bosonic in nature, i.e. triplet and hole–pair excitations. In Ref. 36 a low-energy effective bosonic model has been constructed in which the Gutzwiller constraint of no-double-occupancy is implemented exactly. This is done by projecting out the mode creating particle pair excitations (the so-called π^+ Goldstone

mode) and by retaining only the massless magnon and hole-pair modes. In Ref. 37 we showed that the low-energy SO(5) excitations on the rung of a ladder can be cast into a picture of 5 hard-core bond bosons: three triplet states ($t^\dagger_{\alpha=2,3,4}$) and particle and hole-pair states ($t^\dagger_p$ and $t^\dagger_h$). As an effective coarse-grained model, this description can be extended to three dimensional systems (see also Ref. 38), whereby the excitations are now defined on a 2×2 plaquette[36]. The projection is implemented by restricting within the Hilbert space with $t_p(x) = 0$. The projected SO(5) Hamiltonian takes the form[36]

$$\hat{H} = \Delta_s \sum_{x,\alpha=2,3,4} t^\dagger_\alpha(x) t_\alpha(x) + (\Delta_c - 2\mu) \sum_x t^\dagger_h(x) t_h(x) \qquad (14)$$
$$- J_s \sum_{<xx'>,\alpha=2,3,4} n_\alpha(x) n_\alpha(x') - J_c \sum_{<xx'>} (t^\dagger_h(x) t_h(x') + \text{h.c.}) \,,$$

where $n_\alpha = (t_\alpha + t^\dagger_\alpha)/\sqrt{2}$ are the three components of the Néel order parameter. Δ_s and $\Delta_c \sim U$ are the energies to create a magnon and a hole-pair excitation, respectively, at vanishing chemical potential $\mu = 0$. As one can see, the excitation energy for hole pairs can be compensated by μ in order to have equal energies for spin and hole-pair excitations. Due to this partial compensation, the mean-field ground state of this model[36] recovers exact SO(5) invariance at $J_c = 2J_s$ and $\Delta_s = \Delta_c$.

3.2.1 The pSO(5) Model in Three Dimensions

To explore the physics of Hamiltonian (14) in three dimensions we used the "Stochastic Series Expansion" (SSE) in combination with the loop-operator update as descibed abobe (see Sec. 2). We were able to study systems up to 10^4 sites in three dimensions, including the measurements of arbitrary dynamical response functions.

Figure 5 (left) shows the AF and an SC phase obtained in the 3D calculation, as expected. Furthermore, the two phase transition lines merge into a bicritical point (at $T_b = 0.960 \pm 0.005$ and $\mu_b = -0.098 \pm 0.001$) . The line of equal correlation decay of hole-pairs and triplet bosons also merges into this bicritical point P – a neccessary condition for the restoration of SO(5)-symmetry at this point. The SC phase extends only over a finite μ range; this is due to the hard-core constraint of the hole-pair bosons and agrees with experimentally determined phase diagrams of the cuprates.

T_c and T_N very accurately fulfill the equation $(T_c - T_b)/(T_N - T_b) = 3/2$. This can be interpreted as a first hint suggesting that a large region around the bicritical point is approximately SO(5)-symmetric[12].

A closer look to the phase transition line between the points S and P (see figure 5 middle) reveals that this line is not vertical but slightly inclined: At $T = 0$, the critical chemical potential is $\mu_c = -0.148$ and at $T = T_b$ the value is $\mu_c = \mu_b = -0.098$. This indicates that a finite latent heat is connected with the AF-SC phase transition. Moreover, this means that μ is not a scaling variable for the bicritical point P.

We also calculated the critical exponents and showed that $SO(5)$symmetry is, indeed, asymptotically restored at the bicritical point. A more detailed description can be found in Ref. 39, 12. In real cuprates the ratio between the maximum temperatures T_c and T_N is about 0.17 to 0.25, whereas in the pSO(5) model we obtain the values $T_c/J = 1.465 \pm 0.008$ at $\mu_{opt}/J \approx 1.7$ and $T_N/J = 1.29 \pm 0.01$ at $\mu \to \infty$, hence T_c

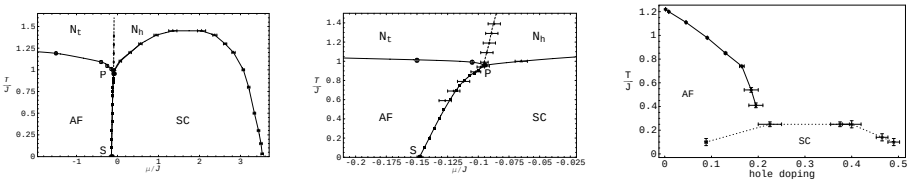

Figure 5. **Left:** Global phase $T(\mu)$ diagram of the three-dimensional pSO(5) model with $J_s = J_c/2$ and $\Delta_s = \Delta_c = J$. N_h is the hole-pair dominated part, N_t the triplet dominated part of the high-temperature phase without long-range order. The separation line between N_h and N_t is the line of equal spatial correlation decay of hole-pairs and bosons. **Middle:** Detailed view to the region near the bicritical point P in the $T(\mu)$ phase diagram of the 3D pSO(5) model. The filled circles with large error bars trace the line of equal decay behavior of the magnon-magnon and the hole pair-hole pair correlation functions. **Right:** Global phase $T(\mu)$ diagram of the "material–adjusted" three-dimensional 4–boson model of Eq. (14), with $J_c : 2J_s = 0.225$ and $\Delta_s = \Delta_c = J$.

is slightly larger than T_N. The correct value of T_c/T_N can be achieved by changing the ratio of $J_c : 2J_s$ from the $SO(5)$symmetric combination to $J_c : 2J_s = 0.225$, as depicted in figure 5 (right). One important question left open here is, whether also the general 4-bosonic model in Eq. 14, with "material adjusted" J_c/J_s–ration, has a $SO(5)$–symmetric behaviour around this critical point P. First numerical studies seem, in fact, to support this conjecture, but further studies are required to be able to make a general statement, i.e, that $SO(5)$ symmetry is dynamically restored at the critical point P.

4 Conclusion

To achieve the above results, in particular to carry out the finite-size scaling related to the critical properties, state of the art numercial simulations have been necessary. We adopted and further developped the Stochastic Series Expansion (SSE), a quantum Monte-Carlo (QMC) algorithm proposed by Sandvik (see Ref. 17 and earlier works referenced therein) for our needs. This algorithm has been enhanced within this project by the considerably implementation of the possible measurement of arbitrary correlation functions (static and time dependend) in the operator-loop update. As already stated above, our implementation of the SSE numerical technique, in combination with the mapping of strongly-correlated fermionic ($t - J$ and Hubbard) models onto effective low-energy bosonic hamiltonians made it possible to simulate up to 10000 lattice sites! Thus within our NIC project, an important achievement was obtained, namely we could simulate for the first time, at least to our knowledge, strongly correlated electron systems in three dimensions in lattices with up to $\mathcal{O}(10^4)$ sites. We consider this as an important break–through in the theory of strongly correlated boson and fermion systems in general. A more detailed description of the algorithm have been published in[18,40].

Using our SSE code, we studied here the phase diagram and the critical exponents of the $pSO(5)$model of high-temperature superconductivityand showed that the $pSO(5)$model captures the essential physics of the cuprates phase diagram. We further showed that even if $SO(5)$symmetry is broken on a microskopic level, $SO(5)$symmetry restores with a transient region around the bicritical point. We refer the interested reader to Ref. 40 where further calculations and details have been discussed.

Acknowledgements

The calculations have been performed at the high performance computing centers in Jülich (ZAM-Jülich) and Munich (LRZ-München). This work was supported by the DFG via a Heisenberg fellowship (AR 324/3-1) and by KONWIHR (OOPCV and CUHE)

References

1. Elbio Dagotto. Correlated electrons in high-temperature superconductors. *Rev. Mod. Phys.*, 66(3):763–840, July 1994.
2. Masatoshi Imada, Atsushi Fujimori, and Yoshinori Tokura. Metal-insulator transitions. *Rev. Mod. Phys.*, 70:1039–1263, 1998.
3. Kazunori Takada, Hiroya Sakurai, Eiji Takayama-Muromachi, Fujio Izumi, Ruben A. Dilanian, and Takayoshi Sasaki. Superconductivity in two-dimensional coo2 layers. *Nature*, 422:53 – 55, 2003.
4. Shou-Cheng Zhang. A unified theory based on SO(5) symmetry of superconductivity and antiferromagnetism. *Science*, 275:1089–1096, 1997.
5. L. Alff, Y. Krockenberger, B. Welter, M. Schonecke, R. Gross, D. Manske, and M. Naito. A hidden pseudogap under the dome of superconductivity in electron-doped high-temperature superconductors. *Nature*, 422:698 – 701, 2003.
6. K. McElroy, R. W. Simmonds, J. E. Hoffman, D. H. Lee, J. Orenstein, H. Eisaki, S. Uchida, and J. C. Davis. Relating atomic-scale electronic phenomena to wave-like quasiparticle states in superconducting $Bi_2Sr_2CaCu_2O_{8+\delta}$. *Nature*, 422:592–596, 2003.
7. Jan Zaanen. Superconductivity: Pebbles in the nodal pond. *Nature*, 422:569–570, 2003.
8. Hirsch. The true colors of cuprates. *Science*, 295:2226, 2002.
9. Subir Sachdev and Shou-Cheng Zhang. Tuning order in cuprate superconductors. *Science*, 295:452–454, 2002.
10. J. G. Bednorz and K. A. Müller. Possible high T_c superconductivity in the ba – la – cu – O system. *Zeit. Phys. B*, 64:189–193, 1986.
11. W. Hanke, A. Muramatsu, and G. Dopf. Das Jülicher Computer–Projekt: Neue Erkenntnisse über die Hochtemperatur–Supraleitung. *Phys. Blätter*, 47:1061–1066, 1991.
12. Ansgar Dorneich. New computational techniques for strongly correlated electron systems. PhD Thesis, Universität Würzburg, 2001.
13. Wolfgang von der Linden. A quantum monte carlo approach to many-body-physics. *Physics Reports*, 220:53–162, 1992.
14. Wolfgang Kinzel and Georg Reents. *Physik per Computer*. Spektrum Verlag, Heidelberg, Berlin, Oxford, 1996.
15. R.H. Landau and M.J. Páez. *Computational Physics*. John Wiley & Sons, New York, 1997.
16. Anders W. Sandvik. Finite-size scaling of the ground-state parameters of the two-dimensional heisenberg model. *Phys. Rev. B*, 56:11678–11690, 1997.
17. A. W. Sandvik. Stochastic series expansion method with operator-loop update. *Phys. Rev. B*, 59(22):R14157–R14160, June 1999.

18. Ansgar Dorneich and Matthias Troyer. Accessing the dynamics of large many-particle systems using the stochastic series expansion. *Phys. Rev. E*, 64:066701, 2001.
19. A. W. Sandvik and J. Kurkijärvi. Quantum monte carlo simulation method for spin systems. *Phys. Rev. B*, 43(7):5950 – 5961, March 1991.
20. A. W. Sandvik. *J. Phys. A*, 25:3667, 1992.
21. W. von der Linden, R. Preuß, and W. Hanke. Consistent application of maximum entropy to quantum monte carlo data. *J. Phys. Condens. Matter*, 8:3881 – 3888, 1996.
22. E. Demler, W. Hanke, and S. C. Zhang. So(5) theory of strongly correlated electron systems. to appear in Rev. Mod. Phys., 2003.
23. C. P. Burgess and C. A. Lutken. SO(5) invariance and effective field theory for high – t_c superconductors. *Phys. Rev. B*, 57:8642–8655, 1998.
24. X. Hu, T. Koyama, and M. Tachiki. Phase diagram of a superconducting and antiferromagnetic system with SO(5) symmetry. *Phys. Rev. Lett.*, 82:2568, 1999.
25. Eugene Demler, Hiroshi Kohno, and Shou-Cheng Zhang. π excitation of the t – J model. *Phys. Rev. B*, 58:5719–5730, 1998.
26. Y. Bazaliy, E. Demler, and S.-C. Zhang. Search for the π resonance in two particle tunneling experiments of YBCO superconductors. *Phys. Rev. Lett.*, 79:1921, 1997.
27. D. P. Arovas, A. J. Berlinsky, C. Kallin, and S.-C. Zhang. Superconducting vortex with antiferromagnetic core. *Phys. Rev. Lett.*, 79:2871–2874, 1997.
28. E. Demler, A. J. Berlinsky, C. Kallin, G. B. Arnold, and M. R. Beasley. Proximity effect and josephson coupling in the so(5) theory of high – tc superconductivity. *Phys. Rev. Lett.*, 80:2917–2920, 1998.
29. Daniel E. Sheehy and Paul M. Goldbart. Intrinsic resistivity and the SO(5) theory of high – temperature superconductors. *Phys. Rev. B*, 57:8131, 1998.
30. D. Goldhaber-Gordon, Hadas Shtrikman, D. Mahalu, David Abusch-Magder, U. Meirav, and M. A. Kastner. Kondo effect in a single – electron transistor. *Nature (London)*, 391:156, Jan. 8 1998.
31. R. Eder, W. Hanke, and S.-C. Zhang. Numerical evidence for SO(5) symmetry and superspin multiplets in the two – dimensional $t--J$ model. *Phys. Rev. B*, 57:13781–13789, 1998.
32. Stefan Meixner, Werner Hanke, Eugene Demler, and Shou-Cheng Zhang. Finite – size studies on the SO(5) symmetry of the hubbard model. *Phys. Rev. Lett.*, 79:4902, 1997.
33. Martin Greiter. Is the π – particle responsible for the 41 meV peak in $YBa_2Cu_3O_7$? *Phys. Rev. Lett.*, 79:4898–4901, 1997.
34. G. Baskaran and P. W. Anderson. On an SO(5) unification attempt for the cuprates. *J. Phys. and Chem. Solids*, 59:1780–1782, 1998.
35. Shou-Cheng Zhang. Recent developments in the so(5) theory of high tc superconductivity. *Journal of Physics and Chemistry of Solids*, 59(10-12):1774–1779, 1998.
36. Shou-Cheng Zhang, Jiang-Ping Hu, Enrico Arrigoni, Werner Hanke, and Assa Auerbach. Projected SO(5) models. *Phys. Rev. B*, 60:13070–13084, 1999.
37. R. Eder, A. Dorneich, M. G. Zacher, W. Hanke, and Shou-Cheng Zhang. Dynamics of an SO(5) symmetric ladder model. *Phys. Rev. B*, 59:561, 1999.
38. Assa Auerbach and Ehud Altman. Projected SO(5) hamiltonian for cuprates and its applications. cond-mat/0009421, 2000.

39. M. Jöstingmeier, A. Dorneich, E. Arrigoni, W. Hanke, and Shou-Cheng Zhang. Scaling properties of the projected SO(5) model in three dimensions. cond-mat/0207528, 2002.
40. Ansgar Dorneich, Martin Jöstingmeier, Enrico Arrigoni, Christopher Dahnken, Thomas Eckl, Werner Hanke, Shou Cheng Zhang, and Matthias Troyer. Object-oriented c++ class library for many body physics on finite lattices and a first application to high-temperature superconductivity. In S. Wagner, W. Hanke, A. Bode, and F. Durst, editors, *Proceedings of the First Joint HLRB and KONWIHR Result and Reviewing Workshop, Garching, Oct. 2002*, Berlin, Heidelberg, New York, 2003. Springer.